

This work was written as part of one of the author's official duties as an Employee of the United States Government and is therefore a work of the United States Government. In accordance with 17 U.S.C. 105, no copyright protection is available for such works under U.S. Law.

Public Domain Mark 1.0

<https://creativecommons.org/publicdomain/mark/1.0/>

Access to this work was provided by the University of Maryland, Baltimore County (UMBC) ScholarWorks@UMBC digital repository on the Maryland Shared Open Access (MD-SOAR) platform.

**Please provide feedback**

Please support the ScholarWorks@UMBC repository by emailing [scholarworks-group@umbc.edu](mailto:scholarworks-group@umbc.edu) and telling us what having access to this work means to you and why it's important to you. Thank you.

# Trajectory modeling of aerosol clouds observed by TOMS

D. R. Allen<sup>1</sup>

National Research Council, Washington, D. C.

M. R. Schoeberl and J. R. Herman

NASA Goddard Space Flight Center, Greenbelt, Maryland

**Abstract.** An aerosol trajectory model (ATM), which couples TOMS aerosol index (AI) measurements with multiple-level parcel trajectories, is presented for determining the three-dimensional (3-D) distribution of a tropospheric aerosol cloud. The ATM is illustrated with an idealized 2-D (height-longitude) cloud in linear vertical shear. The half width of the vertical parcel distribution (an indicator of how well the cloud is resolved) is inversely proportional to time and to vertical shear. The degree to which a cloud can be resolved is limited by an “uncertainty principle,” whereby model precision improves with time, while accuracy degrades with time because of accumulating trajectory errors. ATM is applied to the ash cloud from the September 1992 eruption of Mount Spurr, Alaska. Disagreement in the predicted cloud structure occurs between 3-day ATM runs using United Kingdom Meteorological Office (UKMO) and National Centers for Environmental Prediction (NCEP) winds. This is due to significant differences in the UKMO and NCEP zonal wind speed near the tropopause, which cause large trajectory separations over 3 days. The UKMO-predicted cloud range (310–390 K) agrees well with radar and pilot observations of the ash cloud, while the NCEP-predicted range shows strong disagreement with observations in the region of the jet maximum. This indicates the potential (when independent observations are available) for using ATM to partially validate wind fields.

## 1. Introduction

To completely model the effects of UV-absorbing aerosols on the Earth's radiation budget, global three-dimensional (3-D) aerosol distributions are needed. The Total Ozone Mapping Spectrometer (TOMS) has detected global 2-D (latitude-longitude) distributions of UV-absorbing aerosols using a spectral contrast method [Herman *et al.*, 1997; Torres *et al.*, 1998]. However, to convert the TOMS product (aerosol index (AI) discussed in section 2) to optical thickness, one needs to assume various aerosol properties, including particle size distribution, complex index of refraction, subpixel cloud distribution, and vertical profile [Seftor *et al.*, 1997; Torres *et al.*, 1998]. Errors in each of these factors will propagate through the optical thickness calculation. For example, uncertainty in the height of the aerosol cloud can cause errors of up to 70% in the aerosol optical depth [Torres *et al.*, 1998].

This study explores the possibility of estimating the vertical aerosol profile by coupling TOMS observations with multiple-level isentropic trajectories. In principle, this aerosol trajectory model (ATM) can reconstruct the 3-D shape of the aerosol cloud. However, the trajectories are only as good as the winds used to drive the advection. Therefore this study also involves testing the sensitivity of trajectories to wind errors.

After illustrating the ATM method with an idealized 2-D (height-longitude) cloud in linear vertical wind shear, we apply it to the September 1992 eruption of Crater Peak Vent, Mount

Spurr, Alaska. Trajectory modeling of volcanic ash and SO<sub>2</sub> using TOMS data has been used successfully to model ash transport from Cerro Hudson [Schoeberl *et al.*, 1993], El Chichon [Seftor *et al.*, 1997], and the June 1992 eruptions of Mount Spurr [Shannon, 1996]. This paper builds on previous work by quantifying the degree to which a cloud in given wind shear can be resolved and exploring the sensitivity of predicted cloud height to errors in the winds used to drive the trajectory model. One of the main reasons we chose Mount Spurr (as opposed to a tropical volcano like Pinatubo or El Chichon) is that assimilated midlatitude winds are generally more accurate than tropical winds (see Coy and Swinbank [1997] for a comparison of winds from two data assimilation systems).

In section 2 we discuss the TOMS aerosol index product. Section 3 describes ATM, while section 4 illustrates ATM for an idealized cloud in linear steady shear. Results for the Mount Spurr ash cloud are presented in section 5. The sensitivity to chosen wind field and diabatic heating are discussed along with a comparison of ATM-predicted cloud range to independent radar and pilot reports. Conclusions are provided in section 6.

## 2. TOMS Aerosol Index

TOMS measures aerosol using the two-channel (340 and 380 nm) spectral contrast (or residue) method [Hsu *et al.*, 1996; Herman *et al.*, 1997; Torres *et al.*, 1998]. In the absence of aerosols and clouds the backscattered spectral contrast between 340 and 380 nm is primarily controlled by molecular (Rayleigh) scattering and surface reflection. Mie scattering by aerosols tends to reduce this contrast. A measure of the difference in spectral contrast (defined as aerosol index or AI) is given by

$$AI = -100[\log_{10}(I_{340}/I_{380})_{\text{meas}} - \log_{10}(I_{340}/I_{380})_{\text{calc}}], \quad (1)$$

<sup>1</sup>Now at Department of Geophysical Sciences, University of Chicago, Chicago, Illinois.

Copyright 1999 by the American Geophysical Union.

Paper number 1999JD900763.  
0148-0227/99/1999JD900763\$09.00

where  $(I_{340}/I_{380})_{\text{meas}}$  is the contrast of backscattered radiances measured by TOMS and  $(I_{340}/I_{380})_{\text{calc}}$  is the contrast calculated with a modified version of the *Dave* [1978] Lambert equivalent reflectivity model [McPeters et al., 1996]. AI values larger than at least 0.5 indicate an aerosol content twice the minimum level of detectability, while maximum values can exceed 10 (for AI = 10, the measured ratio is 20% smaller than that predicted from the model). The spectral contrast method is able to detect several types of UV-absorbing aerosols, including volcanic ash [Torres et al., 1995; Seftor et al., 1997], desert dust [Herman et al., 1997], and biomass burning smoke [Hsu et al., 1996].

### 3. Method

The aerosol trajectory model described here couples TOMS column aerosol information with multiple-level trajectories to determine the 3-D aerosol cloud shape. The procedure involves three steps: initialization, advection, and elimination.

#### 3.1. Initialization

Initialization involves choosing a starting date, isolating the aerosol cloud from the background signal, and positioning vertically stacked layers of parcels over the cloud domain. For the volcanic ash cloud studied in this paper we initialize after the eruption has completed. To isolate the cloud from the background, we eliminate data with AI values lower than a specified cutoff value. The cutoff must be large enough to separate the cloud from the background but small enough to keep the bulk of the cloud. For Mount Spurr we choose a cutoff AI of 0.5, which proves sufficient to separate the cloud structure from the background noise for 4 consecutive days. As noted by Herman et al., [1997], AI measurements below 0.5 may be influenced by ground signals, nonabsorbing aerosol, or noise.

When the cloud is isolated from the background, we position vertically stacked layers of parcels over the domain where TOMS observes a large aerosol index (AI > cutoff). The vertical layers are isentropic surfaces ranging from the lowest surface that does not intersect the ground, to an upper surface high enough to encompass the maximum expected cloud height. For Mount Spurr we initialize parcels on 23 levels from 290 to 400 K in 5 K increments. This covers an altitude range from ~3 to 15 km.

#### 3.2. Advection

Parcels are next advected adiabatically with the Goddard Space Flight Center (GSFC) trajectory model [Schoeberl and Sparling, 1995]. This model uses a fourth-order Runge-Kutta time integration scheme with winds interpolated in space and time to the parcel position at each time step (1/100 day time step used in this study). Winds from two meteorological data sets are used for comparison: (1) balanced winds derived from the National Centers for Environmental Prediction (NCEP) analyses [Newman et al., 1988] and (2) United Kingdom Meteorological Office (UKMO) assimilated winds [Swinbank and O'Neill, 1994]. Trajectories are also run in diabatic mode to ascertain the sensitivity of the analysis to diabatic heating.

#### 3.3. Elimination

Parcel elimination involves comparing the horizontal (latitude-longitude) position of each parcel with the TOMS-observed aerosol cloud one or more days after initialization.

Parcels that do not lie within a given great circle radius of a TOMS measurement of large aerosol (AI > cutoff) are eliminated, since they do not track the horizontally projected cloud movement. The great circle radius is chosen to be 200 km, which is the maximum footprint width of the TOMS measurements. Similar estimates (not shown here) for the aerosol cloud profile are obtained with cutoff radii of 150 and 250 km.

The elimination process effectively reconstructs the initial cloud distribution. More precisely, it reconstructs the air mass that tracks the horizontal projection of the aerosol cloud. It is important to note that this method does not provide information on the aerosol density distribution within the cloud but only provides the volume of air likely to contain significant aerosol. (It is possible, using several assumptions, to solve for a best fit to the aerosol density distribution using trajectories and the AI column data. This procedure, however, is much more sensitive to data and trajectory errors than the method described in this paper.)

Finally, we examine the distribution of the number of parcels kept ( $N(\theta_0)$ ) on each isentropic surface, where  $\theta_0$  is the initial potential temperature of the parcel. This quantity is proportional to the volume of air at initialization that tracks the TOMS data on each isentropic level. By comparing  $N(\theta_0)$  from different model runs we can test the model sensitivity to various factors such as choice of wind field and diabatic heating.

### 4. Idealized Cloud Model

To illustrate the technique, we examine an idealized two-dimensional (height-longitude) aerosol cloud placed in a steady zonal wind which increases linearly with altitude. The cloud is initially a rectangle of length  $L_0 = 500$  km and thickness  $D = 2$  km; see shaded region of Figure 1a. When the satellite instrument passes over this cloud it will record aerosol from zero to 500 km, the horizontally projected area of the cloud, which is shown as a thick horizontal line at the bottom of Figure 1a. We initialize parcels across this domain in 0.5-km layers from zero to 10 km. Parcels are placed at 50 km horizontal intervals (the minimum TOMS footprint width) giving 11 parcels at each level. Information on the vertical cloud profile is provided by  $N(z)$ , which is number of parcels at height  $z$  which overlap the aerosol cloud projection. Initially,  $N(z)$  is constant with height, so we have no information on the vertical profile (see Figure 1d).

The parcels are then advected by a steady zonal wind with linear vertical shear:

$$U(z) = U_z \cdot z; \quad U_z = 1 \text{ m s}^{-1} \text{ km}^{-1}; \quad z = 0, 10 \text{ km.} \quad (2)$$

After  $1 \times 10^5$  s (or ~1 day), the parcel column tilts to the right, so some parcels now no longer overlap with the aerosol cloud projection (Figure 1b). These parcels (marked with a cross) are eliminated from the analysis.  $N(z)$  now shows a maximum from 4 to 6 km, with a linear decrease in the “wings” above and below the maximum (Figure 1e). After  $2 \times 10^5$  s (or ~2 days),  $N(z)$  shows a maximum from 4 to 6 km but falls off more sharply in the wings (Figures 1c and 1f).

The degree to which the cloud is vertically resolved can be quantified by the half width  $\delta$  (full width at half maximum) of  $N(z)$ . The time evolution for the half width in this simple case is given by

$$\delta = D + L_0/(U_z t), \quad (3)$$

where  $L_0 = 500$  km and  $D = 2$  km. When  $t = 0$ , the half width is infinite, since we have no information on the vertical

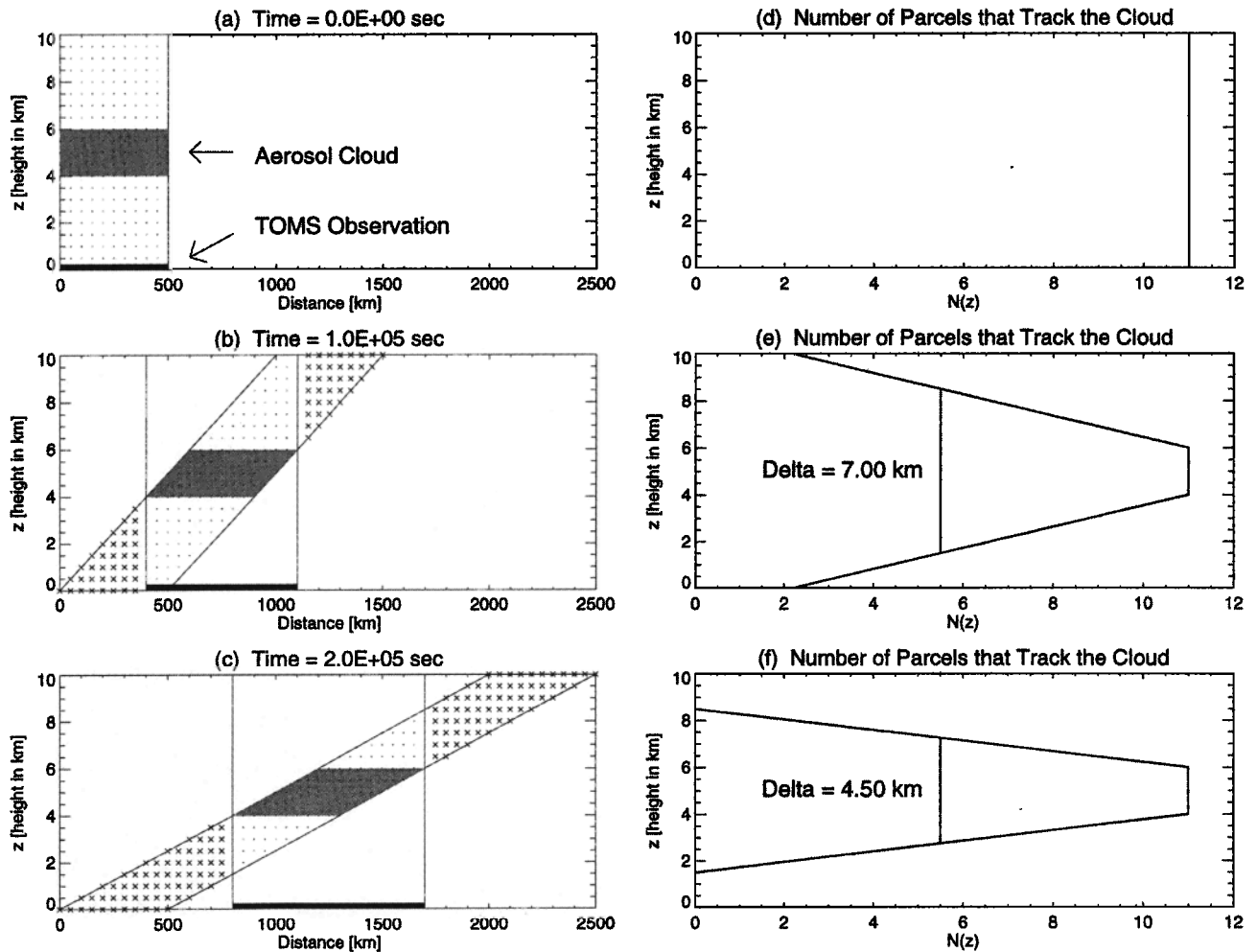


**Figure 1.** Illustration of aerosol trajectory model for two-dimensional (2-D) (longitude-height) cloud in zonal wind with linear vertical shear. (a, b, c) The aerosol cloud (shaded region) is shown at three different times along with the parcels used to model the cloud. Parcels located outside the Total Ozone Mapping Spectrometer (TOMS) observation domain (thick solid line at bottom) are marked with a cross, while parcels inside the column are marked with a point. (d, e, f) Number of parcels  $N(z)$  at each level within the column above the satellite observation. Delta is the half width of the parcel distribution.

profile. As time progresses,  $\delta$  decreases with an inverse time dependence, asymptotically approaching  $D$  for large  $t$ . When  $\delta = D$ , the cloud profile is fully resolved. In Figure 1 we see that  $\delta = 7$  km at  $1 \times 10^5$  s and 4.5 km at  $2 \times 10^5$  s. Since  $\delta - D$  is proportional to  $L_\omega$ , it takes longer to resolve clouds with larger horizontal scale. However,  $\delta - D$  is inversely proportional to  $U_z$ , so strong wind shear allows rapid resolution.

Horizontal trajectory errors will cause errors in the vertical profile  $N(z)$ . For example, suppose a systematic wind error of  $2 \text{ ms}^{-1}$  exists at all levels (i.e.,  $U_{\text{error}} = U_z \cdot z + \varepsilon$ ;  $\varepsilon = 2 \text{ ms}^{-1}$ ). Then the half width will have the same time dependence, but the  $N(z)$  curve will be displaced downward, causing an error in the estimated cloud height of  $\varepsilon/U_z = 2$  km. The technique is also sensitive to random wind errors, which tend to broaden the  $N(z)$  distribution (increasing  $\delta$ ) without shifting the location of the maximum  $N(z)$ . As the scale of the random trajectory errors approaches the same order as the horizontal scale of the cloud, then the width of the distribution becomes very large, thereby contaminating the estimated cloud height. A discussion of trajectory errors for the Mount Spurr case study is included in section 5.

## 5. Tracking the Mount Spurr Ash Cloud

### 5.1. TOMS Observations of the Ash Cloud

To test the aerosol trajectory model, we estimate the ash cloud distribution from the September 1992 eruption of Mount Spurr, Alaska. The Crater Peak vent, Mount Spurr volcano eruptions of June, August, and September 1992 combined to release some 150 million  $\text{m}^3$  of tephra into the atmosphere, reaching altitudes of nearly 15 km above sea level [Eichelberger et al., 1995; Krotkov et al., 1999]. The third major eruption, which is used for the case study here, started at 1203 Alaskan daylight time on September 17 and lasted about 3.5 hours [Alaska Volcano Observatory, 1993]. A large cloud of ash [Schneider et al., 1995] and  $\text{SO}_2$  [Bluth et al., 1995] was injected into the upper troposphere.

The location of the volcanic aerosol (ash) cloud as observed from TOMS level-2 aerosol index data (where  $\text{AI} > 0.5$ ) on four consecutive days is shown in Figure 2. The cloud initially drifted eastward into Canada followed by strong southward advection into the United States. It then turned eastward, crossing the lower Great Lakes region. From September 18 to

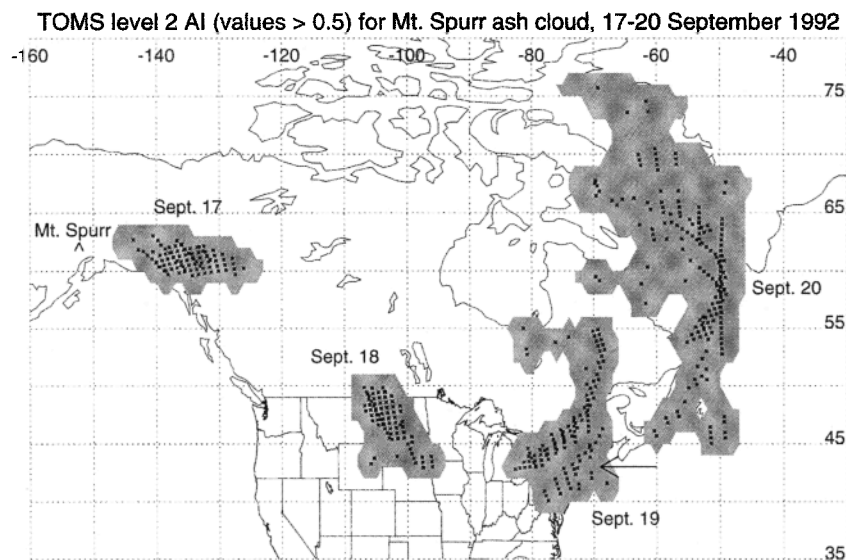


**Figure 2.** Location of the Mount Spurr ash cloud is identified here in TOMS level-2 data. The points indicate the positions of the TOMS measurements of AI > 0.5 from September 17 to 20, 1992. The shaded region provides a rough sketch of the domain that lies within 200-km great circle radius of the TOMS measurements.

19 it entered a region of strong horizontal and vertical shear that stretched the cloud into a thin arc with cyclonic curvature from south to north. (Note that the secondary feature to the south on September 19 (see arrow) has unknown origin. It was not observed in either advanced very high resolution radiometer (AVHRR) or TOMS SO<sub>2</sub> data, and is not well tracked by the trajectory runs discussed in this paper). By September 20 the cloud moved northeastward arcing from Baffin Island (70°W, 68°N) to the southern tip of Greenland, to Newfoundland (55°W, 48°N).

The 0.5 AI cutoff used in Figure 2 eliminates most of the background aerosol. However, on each day there are some outlying individual measurements with AI > 0.5 (for example, the secondary feature noted above, the measurements near 80°W, 55°N on September 19, and the high-latitude measurements near 75°N on September 20). Since none of the trajectories initialized on September 17 track into these outlying regions, the inclusion of these outlying measurements does not cause problems in the following analysis.

## 5.2. Horizontal Tracking by Trajectory Model

A column of parcels is initialized over each level 2 measurement shown for September 17. TOMS made 91 measurements of AI > 0.5 on September 17, so 91 columns were initialized. Parcels were placed at every 5 K from 290 to 400 K, roughly from the top of Mount Spurr (~3 km) to 15 km, spanning the expected ash cloud range. The TOMS observations on September 17 are a composite from three consecutive satellite orbits, where each orbit is separated in time by about 90 min. Therefore we initialize three sets of parcel columns at the precise times the observations were made. This asynoptic initialization is important when modeling fast-moving clouds. For example, with wind speeds of 30 m s<sup>-1</sup>, parcels will travel 162 km in 90 min. This may be significant for the Mount Spurr case, since the horizontal scale of the cloud initially ~1000 km (east-west) by 500 km (north-south).

Each parcel was advected adiabatically for 3 days using the GSFC trajectory model [Schoeberl and Sparling, 1995]. Isen-

tropic trajectories were run separately with NCEP and UKMO horizontal winds. On September 20 (after a 3-day trajectory run), the horizontal parcel positions were compared with the TOMS data shown in Figure 2. Parcels were kept that fell within 200 km great circle radius of the TOMS data at the time the TOMS observations were made, while parcels lying outside the 200 km radius were eliminated. The domain within a 200-km great circle of the TOMS measurements is illustrated by the shaded region in Figure 2.

Plate 1 shows the parcels kept for the NCEP and UKMO runs on four consecutive days. The parcels are color-coded by potential temperature, with the lowest potential temperatures plotted first, overlaid by upper layers. Plate 1 basically shows the cloud as seen from above, since lower regions may be hidden from view. Parcel locations are plotted synoptically once per day; note that these synoptic “snapshots” are not directly comparable to the asynoptic nature of the TOMS data in Figure 2.

A comparison of the two cases in Plate 1 shows the sensitivity of the trajectories to chosen wind field. On September 17 the NCEP and UKMO runs show the eastern half of the cloud attaining higher theta values than the western half, indicating an upward and eastward tilting of the cloud top. On September 18 both runs track the main portion of the cloud into the United States and southern Canada with a low potential temperature tail trailing northward. The general northwest-southeast horizontal orientation of the clouds agrees with the TOMS observations in Figure 2. Many of the UKMO parcels extend farther south than the NCEP parcels, indicating stronger UKMO southerly winds.

By September 19 the effect of strong wind shear is seen by the stretching of the clouds into a long arc, similar to the TOMS observations. The shapes of the arcing clouds, however, are quite different. The NCEP parcels are contained in two distinct cloud layers. The upper layer from 345 to 395 K (red, yellow, and green parcels) stretches northeastward from the Great Lakes to 67°W, 58°N, downward from northwest to

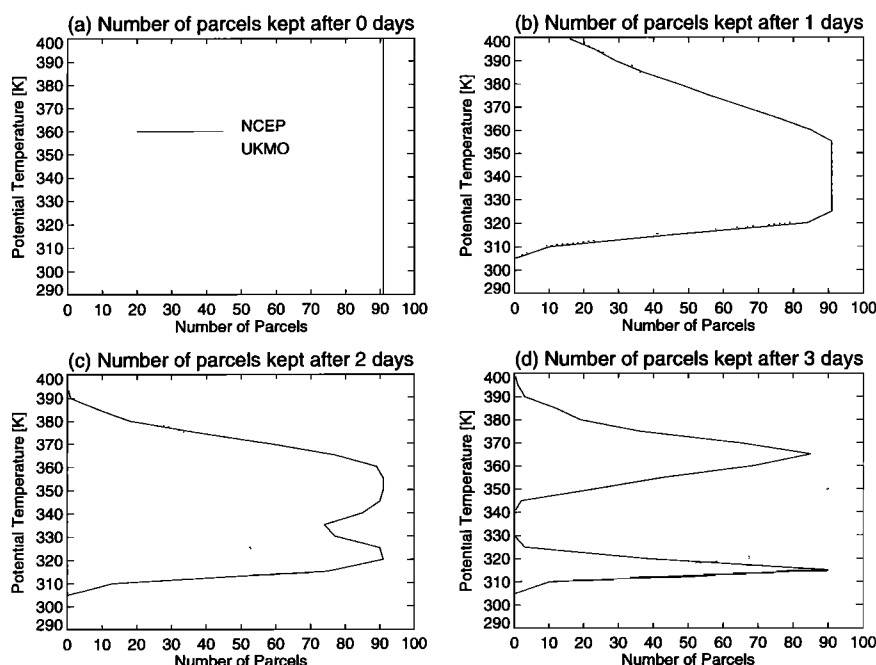


**Figure 3.** Number  $N(\theta_o)$  of NCEP and UKMO parcels (out of 91) kept at each level after (a) 0-, (b) 1-, (c) 2-, and (d) 3-day trajectories.

southeast. The lower layer from 310 to 325 K (purple parcels) is oriented almost east-west along the 47°N latitude line. A gap from 330 to 340 K occurs between the two clouds where no parcels are able to track the TOMS observations (discussed further below).

In comparison, the UKMO cloud top on September 19 has a similar downward tilt from northwest to southeast. However, the UKMO data show a broader cloud on September 19 with less extension into northeastern Canada. The main portion of the cloud is positioned several degrees south of the NCEP cloud, with the southern edge reaching 40°N. Note that none of the parcels from these runs track the secondary southerly feature observed in TOMS AI on September 19 (see arrow on Figure 2). On September 20, cyclonic arcing from south to north is seen in both trajectory runs. The NCEP and UKMO clouds roughly overlap, but NCEP shows a broader cloud that tilts steeply downward and eastward from 395 to 310 K, while UKMO shows a more uniform cloud top.

### 5.3. Vertical Distribution of Parcels

The qualitative comparison above shows that the estimated cloud structure for the Mount Spurr case is sensitive to the meteorological wind field analysis used. Here we quantify the sensitivity of estimated cloud height by examining the number of parcels kept at each potential temperature level,  $N(\theta_o)$ . Estimates of the ash cloud height are given by the potential temperature range of the maxima in  $N(\theta_o)$ .

Figure 3 shows  $N(\theta_o)$  for the NCEP and UKMO trajectory runs. Here the parcel positions are compared with the TOMS data after 0, 1, 2, and 3 days. Parcels within 200 km of a TOMS observation on the specified day are kept, while those outside 200 km were eliminated. This figure illustrates the increasing discrepancy between the NCEP and UKMO analyses for longer trajectory runs; 1- and 2-day trajectory runs show fairly good agreement. However, for the 3-day trajectory run the NCEP  $N(\theta_o)$  shows a bimodal structure with peaks at 315 and

365 K, while UKMO  $N(\theta_o)$  is a broad unimodal distribution, maximizing at 350 K. Interestingly, from 330 to 340 K, none of the NCEP parcels are able to track the TOMS observations, compared to more than half of the UKMO parcels. By comparing individual wind profiles for NCEP and UKMO it was found that the NCEP jet (which maximizes near 330 K) is about  $3\text{--}4\text{ ms}^{-1}$  stronger than the UKMO jet. This causes the NCEP parcels to be advected well to the east of the UKMO parcels after three days.

To further examine this discrepancy, we show histograms of the longitude of NCEP and UKMO parcels at 340 K for 1-, 2-, and 3-day trajectories (see Figure 4, top). At initialization (not shown) the histograms are identical. After one day it is clear that the two histograms are separating with the NCEP parcels being advected farther eastward. After two days, only the wings of the histograms overlap, while after three days, the histograms do not overlap at all, and their mean longitudes are separated by more than  $10^\circ$ .

To quantify the degree of separation between the NCEP and UKMO longitude histograms, we define a separation factor  $S(\theta, \text{time})$ :

$$S = \frac{M_{\text{NCEP}} - M_{\text{UKMO}}}{\sigma_{\text{NCEP}} + \sigma_{\text{UKMO}}}, \quad (4)$$

where  $M$  is the mean and  $\sigma$  is the standard deviation of the longitude histograms. For  $S > 1$ , the UKMO and NCEP longitude histograms are significantly separated, and therefore we expect different results for the estimated aerosol cloud structure. Figure 4 (bottom) shows how the separation factor changes with time. After 3 days,  $S > 1$  from 300 to 360 K. These large separations account for the large differences in  $N(\theta_o)$  shown in Figure 3d. Assuming that this parcel separation is due to systematic wind errors, we infer that the resulting 3-day trajectory errors may be too large to make a reliable estimate of cloud height. To reduce the uncertainties, we need to use shorter trajectories.

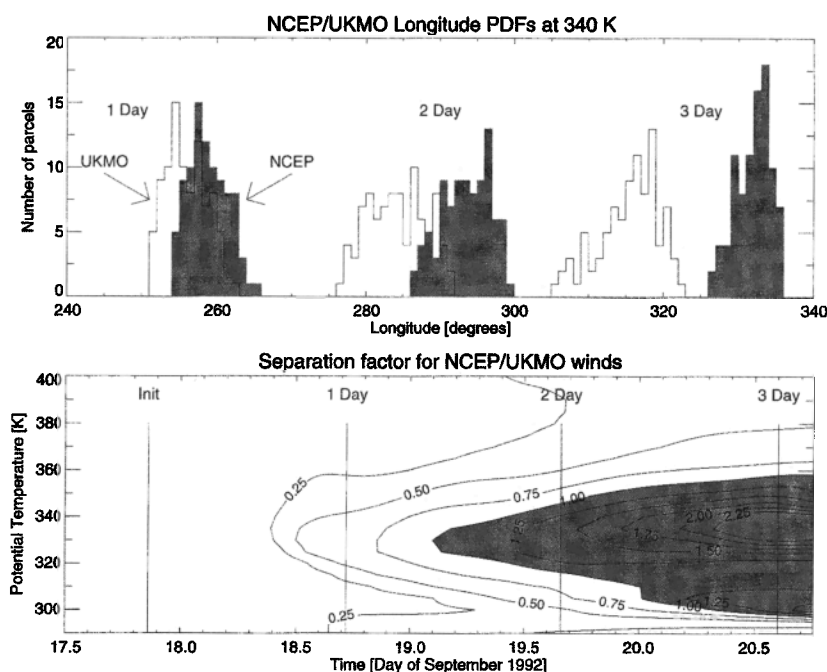


**Figure 4.** (top) Histograms are plotted for the longitude of the NCEP and UKMO parcel ensembles at 340 K. The three plots show the distributions after 1-, 2-, and 3-day trajectories. (bottom) The separation factor  $S$  defined in equation (4). Small  $S$  indicates mostly overlapping NCEP and UKMO distributions, while large  $S$  indicates a strong separation between the distributions.

Changing from 3-day to 2-day trajectories does reduce the separation factor, as shown in Figure 4, bottom. However,  $S$  is still greater than 1 over the range 315–345 K. Reducing to 1-day trajectories gives a smaller separation factor ( $S < 1$  everywhere) and better alignment of the  $N(\theta_o)$  (see Figure 3b). By reducing the length of the trajectories we obtain better agreement between the  $N(\theta_o)$  calculated with the different wind fields. However, this gain was at the expense of reduced resolution of the cloud peak. This result is consistent with (3), which states that the half width of  $N(\theta_o)$  increases with decreased time.

To further quantify the trajectory errors, we examine the great circle distance between the center of mass (CM) of

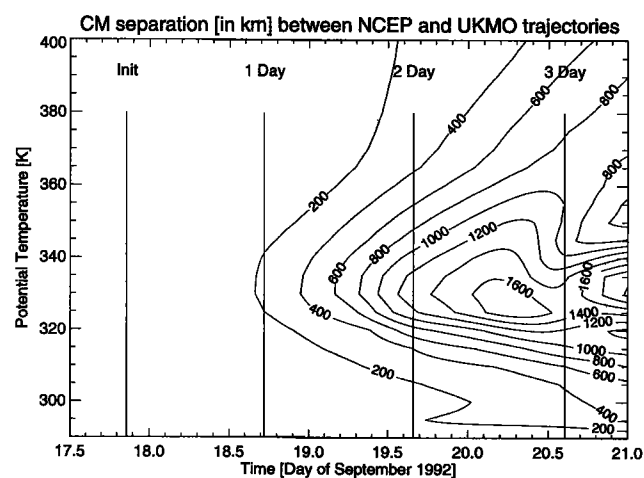


**Figure 5.** Great circle distance (in kilometers) between the centers of mass of NCEP and UKMO parcel ensembles as a function of potential temperature and time.

NCEP and UKMO parcel ensembles at each level (see Figure 5). The CM distance gives a measure of the difference in average parcel position due to time-integrated NCEP and UKMO wind differences. After one day the CM separation is less than 200 km, except from 330 to 340 K, at the jet maximum. From one to two days the separation increases at all levels except 290 K, with values now ranging from 100 to over 1200 km. After three days, separations of nearly over 1600 km are found near 330 K. We can use these values to estimate the time-integrated difference in the NCEP and UKMO winds. Separations of 500 to 1600 km in 3 days translate to wind differences of 2 to 6 m s<sup>-1</sup>. In another calculation (not shown here) we found that the separation rates of individual parcel pairs (which were initialized identically but advected with two different winds) near 330 K are close to the CM separation rates. This is another indication that a large systematic wind bias exists between the NCEP and the UKMO data. These results are consistent with *Pickering et al.*, [1994] who observed large differences in isentropic trajectories in the troposphere (over southern Africa and the South Atlantic) calculated with meteorological fields from different analysis centers. Mean separations of up to 2500 km were observed for 8-day trajectory runs, indicating significant discrepancies between the two analysis fields.

The preceding analysis illustrates an essential problem of ATM: how to balance precision and accuracy to obtain the best estimate of the cloud height. ATM requires a long enough time integration to allow the shear to do its job in resolving the cloud peak (see (3)). However, as time progresses, the trajectory errors increase, thereby reducing the accuracy of the analysis. This “uncertainty principle” limits how well we can model the aerosol clouds. Handling of such errors will of course be case-specific, since trajectories vary significantly depending on the flow pattern. For the Mount Spurr case, large errors occur

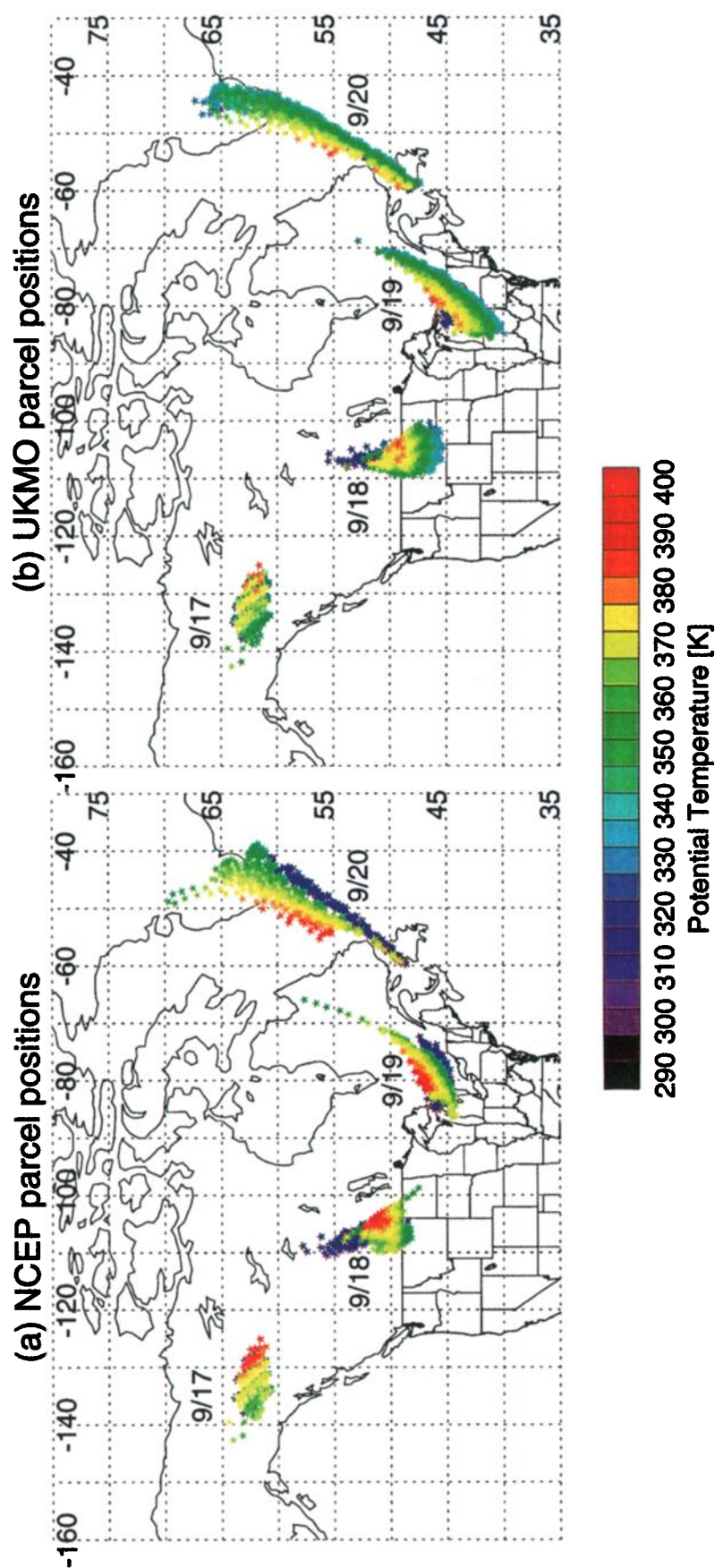


**Plate 1.** (a) National Centers for Environmental Prediction (NCEP) and (b) United Kingdom Meteorological Office (UKMO) parcel locations for four consecutive days. Only parcels that lie within 200 km of a TOMS measurement with  $AI > 0.5$  on September 20 are plotted. Parcels are color-coded by potential temperature.

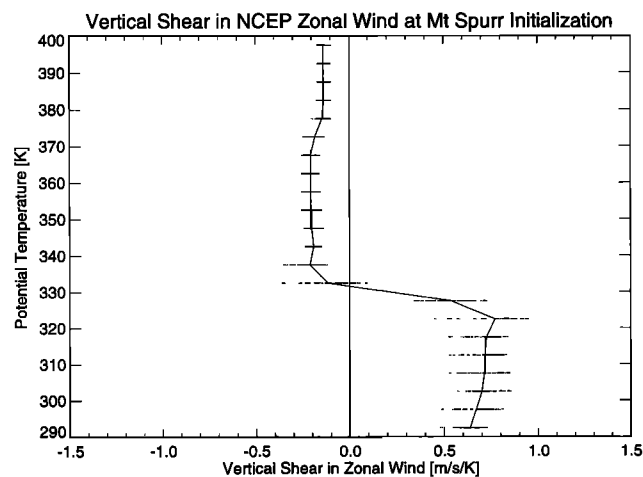


**Figure 6.** Vertical shear in NCEP zonal wind at initialization for the Mount Spurr trajectory analysis. The wind shear is plotted at the location of each parcel (dots) along with the shear averaged over all parcels at each level (solid line).

over three days, being of the same order as the length scale of the ash cloud. To obtain more accurate estimates of the cloud shape, we could reduce the length of the trajectories. This would provide increased stability of the model at the expense of weaker resolution of the cloud height.

#### 5.4. Effects of Vertical Wind Shear

To use the ATM to estimate the ash cloud height, it is important not only to consider trajectory errors but also to examine how the vertical distribution of wind shear affects the resolving capability of the model. According to (3) the slope of the  $N(z)$  curve (which is proportional to  $\delta - D$ ) is inversely proportional to the vertical wind shear. If the wind shear varies with height, then the resolving capability of the model will also vary with height. To illustrate this relationship, we first suppose that the wind shear along the parcel path does not change much over the first day of the trajectory runs. Figure 6 shows a profile of the NCEP wind shear at initialization (note that here we show the vertical shear  $du/d\theta$ , with potential temperature as the vertical coordinate). The shear at each individual parcel location is plotted along with the ensemble average at each potential temperature (solid line). Below the jet maximum (near 330 K) the shear is roughly a constant  $0.7 \text{ m s}^{-1} \text{ K}^{-1}$ , while above the maximum, it is roughly a constant  $-0.2 \text{ m s}^{-1} \text{ K}^{-1}$ . So the magnitude of the wind shear is  $\sim 3.5$  times stronger below the jet maximum. This is consistent with the different slopes of the NCEP 1-day  $N(\theta_0)$  curve in Figure 3b. The lower “wing” of the  $N(\theta_0)$  drops off rapidly below 320 K, while the upper wing has a much slower drop-off. By calculating the ratio of the magnitude of the slopes it is found that the lower wing drops off  $\sim 3.5$  times faster than the upper wing, similar to the ratio of the wind shears.

It is clear from this analysis that the ability of the trajectory model to resolve the vertical cloud structure is limited by the wind shear. In the strong shear zone (below 330 K) the cloud is resolved 3.5 times faster than in the weak shear zone (above 330 K). This tends to bias the  $N(\theta_0)$  distribution toward the weak shear zone, since fewer parcels are eliminated there. If we calculate vertical shear with geometric height  $z$ , rather than potential temperature, we find that the situation is not so bad

as it seems. Since the static stability (proportional to  $d\theta/dz$ ) is about 3 times larger above the jet maximum, then the magnitude of the wind shear with altitude,  $|du/dz| = |du/d\theta| (d\theta/dz)$ , is roughly the same above and below 330 K. So although we have differential model resolution with potential temperature, the resolution with geometric height is roughly uniform.

For a general flow field it may prove difficult to account for varying vertical wind shear. If the wind is steady, one could simply run the parcels in weaker shear zones for longer times to obtain equal resolution. However, as mentioned above, accumulating trajectory errors will eventually contaminate the  $N(\theta_0)$  distribution. For time-varying flow patterns, the problem further requires analysis of wind shear along the parcel path (i.e., in the Lagrangian framework). More work is necessary in order to develop a robust correction technique for differential resolving capability of the ATM.

#### 5.5. Diabatic Effects on Parcel PDFs

The isentropic trajectory model described above neglects the effects of diabatic heating/cooling of the air mass containing the aerosol as well as the heating of the cloud by aerosol absorption of infrared surface radiation. Trajectory errors due to neglect of diabatic effects will be of the order of

$$E = \frac{du}{d\theta} H(\Delta t)^2, \quad (5)$$

where  $H = d\theta/dt$  is the diabatic heating rate and  $\Delta t$  is the time elapsed for the given trajectory. Heating rates provided by Rosenfield [1994] show  $H$  generally less than  $1 \text{ K/d}$  for the region considered in the Mount Spurr case. For wind shears of  $0.5 \text{ m s}^{-1} \text{ K}^{-1}$  we estimate maximum trajectory errors of about 400 km after three days. On September 20 we find the east-west scale of the cloud to be at least 1000 km. The maximum trajectory errors from neglect of diabatic effects are therefore less than the horizontal scale of the cloud but could still cause errors in the ATM-predicted cloud height.

For a more rigorous test of diabatic effects we ran the trajectory model in diabatic mode, in which the Rosenfield [1994] heating rates were used to displace the parcels from constant potential temperature surfaces. Figure 7 shows that the UKMO  $N(\theta_0)$  from diabatic runs deviates only slightly from the 1-, 2-, and 3-day adiabatic trajectories except below 320 K, where significant heating rates combine with large shear to cause trajectory errors of over 1000 km. Including diabatic effects does not significantly alter the estimation of cloud height for this case. However, for cases involving longer trajectory runs or regions of large diabatic heating/cooling, the inclusion of diabatic effects may be important for the success of ATM. For a more detailed discussion of diabatic effects on trajectories the reader is referred to Morris *et al.*, [1995].

#### 5.6. Comparison With Radar and Pilot Reports

To fully validate the ATM, it is essential to compare the estimated cloud range with independent observations. It is not valid to conclude that since trajectories at a given level do a good job tracking the cloud, then the height of the cloud is known. As illustrated in section 4, systematic wind errors will shift the  $N(\theta_0)$  distributions, so the best agreement with horizontal position occurs at the wrong level. Fortunately, for the Mount Spurr eruption, radar estimates [Rose *et al.*, 1995] and pilot reports [Casadevall and Krohn, 1995] are available for independent verification of model results.

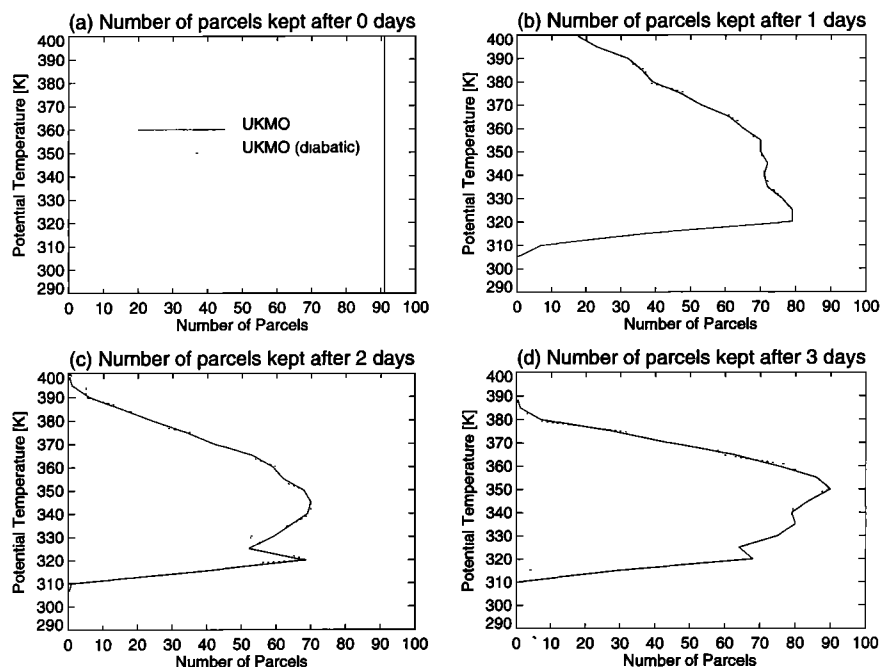


**Figure 7.** Number of UKMO parcels kept for adiabatic (solid) and diabatic (dashed) trajectory runs.

A C-band radar was installed at Kenai, Alaska, just prior to the 1992 Mount Spurr eruptions. This radar provided real-time ash cloud tracking near the volcano. The data were used as input for forecasting models. The radar-observed cloud extended from  $\sim 3$  to 15 km altitude (similar to the range predicted by the UKMO trajectories; see discussion of Plate 2 below). A large fraction of this ash would be expected to fall out from gravitational settling in a nearby radius around the volcano. The remaining airborne ash was transported by the prevailing winds.

A compilation of pilot reports was made by the NOAA Synoptic Analysis Branch and published by *Casadevall and Krohn* [1995]. These cover a broad range of the cloud paths over Alaska, southern Canada, and the continental United States. Plate 2 shows the pilot observations of cloud base ( $B$ ) and top ( $T$ ) as a function of latitude and pressure, placed over contours of NCEP-derived zonal mean potential temperature on September 18, 1992. The colored dots indicate positions of UKMO-derived trajectories that were kept for the 3-day run (see Figure 3d). Parcel locations are plotted for September 17 (red), 18 (green), 19 (blue), and 20 (yellow). The altitude scale is calculated with a log-pressure relationship and scale height of 7.6 km. Except for four low-altitude observations made near the volcano (bottom right of Plate 2), the pilot reports are concentrated from 305 to 355 K. The lowest and highest altitudes recorded for this range were 3.5 and 12.7 km. The number of cloud top observations falls off rapidly above about 11.4 km ( $\sim 355$  K). It is possible that the ash cloud at the times of the pilot reports does not extend above this level, since the larger particles observed by radar may gravitationally settle from the lower stratosphere to the troposphere. However, it is also likely that the vertical extent of the pilot reports is limited by the maximum altitudes obtained by commercial aircraft, since the pilots would have to be at the level of the cloud height to make an accurate observation. Also, the pilots may have difficulty visually identifying the aerosol clouds at higher altitudes due to decreasing density and smaller particle size. For

these two reasons, the pilot observations shown here may underestimate the maximum height of the ash cloud.

Both the UKMO and the NCEP 3-day trajectory runs predict a cloud base near 305 K, close to the lowest pilot observations. The NCEP-predicted top of 400 K is  $\sim 35$ – $45$  K ( $\sim 3$  km), higher than maximum pilot report, but within 1–2 km of the radar-predicted cloud top of 15 km. It appears the NCEP trajectories from 330 to 340 K are in error, since the NCEP  $N(\theta_0)$  predicts no ash in this range after three days (Figure 3d), while pilot reports indicate a definite ash presence. As mentioned, the NCEP tropospheric jet is  $3\text{--}4\text{ m s}^{-1}$  stronger than the UKMO jet. This strong jet pushes parcels in the 330 to 340 K region well east of the TOMS aerosol observations on September 20.

The UKMO  $N(\theta_0)$  does a better job of spanning the range of maximum pilot observations from 305 to 355 K. The UKMO parcel locations shown in Plate 2 overlap nearly all the pilot reports, indicating a reliable capture of the cloud evolution. The parcels reach a maximum altitude of 15 km, consistent with radar observations. This supports the idea that pilot reports underestimate the cloud top by  $\sim 2$  km. This case study illustrates the potential of using ATM with independent observations of cloud height for partial validation of winds used to drive the trajectories. The UKMO-assimilated wind field for this time period provides good tracking of the ash cloud, while the NCEP-derived balanced winds appear to be  $\sim 5\text{ m s}^{-1}$  too strong in the region of the jet maximum.

## 6. Conclusions

This study examines the feasibility of reconstructing the distribution of an aerosol cloud by coupling a trajectory model with TOMS column aerosol observations. The precision and accuracy of the model depend strongly on the ambient wind shear and trajectory errors. As parcel trajectories are run for longer times, wind shear separates parcels horizontally, allowing the location of the aerosol cloud to be more precisely

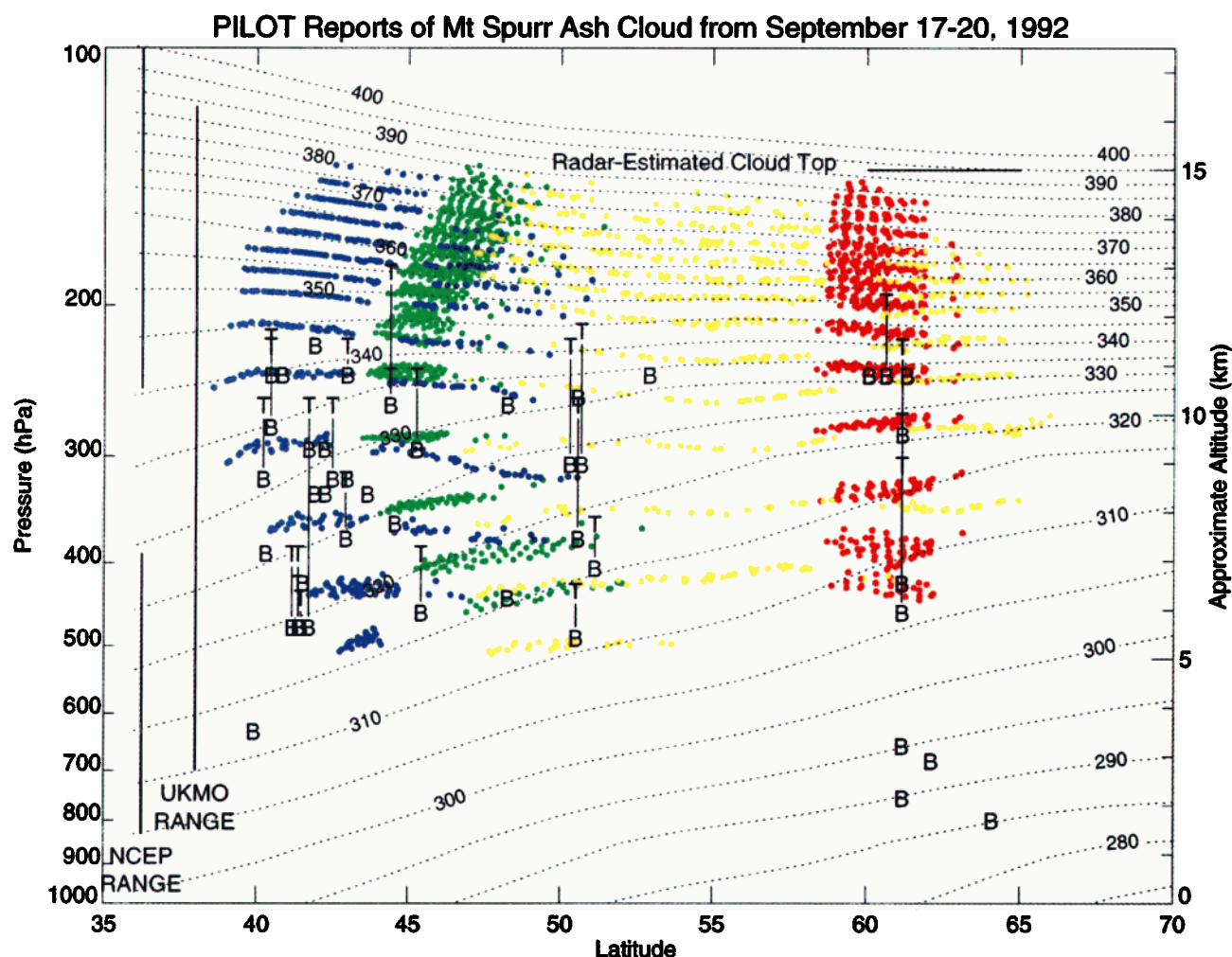


**Plate 2.** Observed and ATM-predicted Mount Spurr ash cloud height ranges plotted over the zonal mean NCEP potential temperature on September 18, 1992. Pilot reports are indicated by base (B) and/or top (T), which are connected with a line if both are present. The radar estimate of cloud top is shown at 15 km along with the predicted ranges from the UKMO and NCEP trajectory analyses. UKMO parcel locations are plotted for September 17 (red), 18 (green), 19 (blue), 20 (yellow).

defined. However, trajectory errors accumulate with time, thereby decreasing the accuracy of the model. This leads to an “uncertainty principle” that limits how well a given cloud can be resolved. We also found that the resolving capability of the model varies in regions of differential vertical shear. The cloud shape can be discerned faster in strong shear regions than in weak shear regions. This further complicates the interpretation of the results of the model. To obtain reliable quantitative cloud height estimates from the model, a balance among precision, accuracy, and differential shear must be achieved.

The September 1992 Mount Spurr ash cloud provided a good test case. The vertical profile of the number of parcels tracking the horizontal projection of the cloud ( $N(\theta_o)$ ) was shown to be insensitive to diabatic heating but quite sensitive to the choice of meteorological wind field for 2-day and 3-day trajectory runs. The NCEP and UKMO trajectories near the tropospheric jet maximum deviated by over 1600 km after three days, indicating systematic wind differences of up to  $6 \text{ m s}^{-1}$  averaged over the Lagrangian parcel paths. Much better agreement was obtained with 1-day trajectories, at the expense of reduced vertical resolution of the cloud structure. The UKMO-estimated range of 310–390 K ( $\sim 5 - 15 \text{ km}$ ) is in

good agreement with radar and pilot reports of the ash cloud height, while the NCEP trajectories failed to track the aerosol cloud near the jet maximum.

This result indicates the potential of using aerosol trajectory modeling not only for estimating the cloud structure but also as a tool for partially validating meteorological wind fields. When independent vertical information for the ash cloud is available, the trajectory model provides a stringent test, which can help quantify the accuracy of various wind fields.

**Acknowledgments.** This paper benefited from conversations with the TOMS aerosol group and Lynn Sparling at NASA GSFC. We appreciated the helpful reviews provided by Gary Morris and Gregg Bluth. This work was performed while D. Allen held a National Research Council/NASA GSFC Research Associateship.

## References

- Alaska Volcano Observatory, Mt. Spurr's 1992 eruptions, *Eos Trans. AGU*, 74(19), 217–224, 1993.
- Bluth, G. J. S., C. J. Scott, I. E. Sprod, C. C. Schnetzler, A. J. Krueger, and L. S. Walter, Explosive emissions of sulfur dioxide from the 1992 Crater Peak Eruptions, Mount Spurr Volcano, Alaska, in *The 1992*

- Eruptions of Crater Peak Vent, Mount Spurr Volcano, Alaska, U.S. Geol. Surv. Bull., B-2139*, 37–45, 1995.
- Casadevall, T. J., and M. D. Krohn, Effects of the 1992 Crater Peak eruptions on airports and aviation operations in the United States and Canada, in *The 1992 Eruptions of Crater Peak Vent, Mount Spurr Volcano, Alaska, U.S. Geol. Surv. Bull., B-2139*, 205–220, 1995.
- Coy, L., and R. Swinbank, Characteristics of stratospheric winds and temperatures produced by data assimilation, *J. Geophys. Res.*, **102**, 25, 763–25, 781, 1997.
- Dave, J. V., Effect of aerosols on the estimation of total ozone in an atmospheric column from the measurement of its ultraviolet radiance, *J. Atmos. Sci.*, **35**, 899–911, 1978.
- Eichelberger, J. C., T. E. Keith, T. P. Miller, and C. J. Nye, 1992 eruptions of the Crater Peak vent of Mount Spurr volcano: Chronology and summary, in *The 1992 Eruptions of Crater Peak Vent, Mount Spurr Volcano, Alaska, U.S. Geol. Surv. Bull., B-2139m*, 1–18, 1995.
- Herman, J. R., P. K. Bhartia, O. Torres, C. Hsu, and E. Celarier, Global distribution of UV-absorbing aerosols from Nimbus 7/TOMS data, *J. Geophys. Res.*, **102**, 16,911–16,922, 1997.
- Hsu, N. C., J. R. Herman, P. K. Bhartia, C. J. Seftor, O. Torres, A. M. Thompson, J. F. Gleason, T. F. Eck, and B. N. Holben, Detection of biomass burning smoke from TOMS measurements, *Geophys. Res. Lett.*, **23**, 745–748, 1996.
- Krotkov, N. A., et al., Comparison of TOMS and AVHRR volcanic ash retrievals from the August 1992 eruption of Mt. Spurr, *Geophys. Res. Lett.*, **26**, 455–458, 1999.
- McPeters, R. D., et al., Nimbus 7 total ozone mapping spectrometer (TOMS) data products users guide, *NASA Ref. Publ.*, **1384**, 1996.
- Morris, G. A., et al., Trajectory mapping and applications to data from the Upper Atmosphere Research Satellite, *J. Geophys. Res.*, **100**, 16,491–16,505, 1995.
- Newman, P. A., et al., Meteorological atlas of the Southern Hemisphere lower stratosphere for August and September 1987, *NASA Tech. Memo.*, **4049**, 1–131, 1988.
- Pickering, K. E., A. M. Thompson, D. P. McNamara, and M. R. Schoeberl, An intercomparison of isentropic trajectories over the South Atlantic, *Mon. Weather Rev.*, **122**, 864–879, 1994.
- Rose, W. I., A. B. Kostinski, and L. Kelley, Real time C-band radar observations of 1992 eruption clouds from Crater Peak vent of Mount Spurr, Alaska, in *The 1992 Eruptions of Crater Peak Vent, Mount Spurr Volcano, Alaska, U.S. Geol. Surv. Bull., B-2139*, 19–26, 1995.
- Rosenfield, J. E., P. A. Newman, and M. R. Schoeberl, Computations of diabatic descent in the stratospheric polar vortex, *J. Geophys. Res.*, **99**, 16,677–16,689, 1994.
- Schneider, D. J., W. I. Rose, and L. Kelley, Tracking of 1992 eruption clouds from the Crater Peak vent of Mount Spurr volcano, Alaska, using AVHRR, in *The 1992 Eruptions of Crater Peak Vent, Mount Spurr Volcano, Alaska, U.S. Geol. Surv. Bull., B-2139*, 27–36, 1995.
- Schoeberl, M. R., and L. C. Sparling, Trajectory modeling, in *Diagnostic Tools in Atmospheric Physics, Enrico Fermi, Course CXVI*, edited by G. Fiocco and G. Visconti, pp. 289–305, North-Holland, New York, 1995.
- Schoeberl, M. R., S. D. Doiron, L. R. Lait, P. A. Newman, and A. J. Krueger, A simulation of the Cerro Hudson SO<sub>2</sub> cloud, *J. Geophys. Res.*, **98**, 2949–2955, 1993.
- Seftor, C. J., N. C. Hsu, J. R. Herman, P. K. Bhartia, O. Torres, W. I. Rose, D. J. Schneider, and N. Krotkov, Detection of volcanic ash from Nimbus 7/total ozone mapping spectrometer, *J. Geophys. Res.*, **102**, 16,749–16,759, 1997.
- Shannon, J. M., The 3-D reconstruction of the Mt. Spurr volcanic clouds using AVHRR, TOMS, and wind trajectory data, 95 pp., M.S. thesis, Mich. Technol. Univ., Houghton, 1996.
- Swinbank, R., and A. O'Neill, A stratosphere-troposphere data assimilation system, *Mon. Weather Rev.*, **122**, 686–702, 1994.
- Torres, O., J. R. Herman, P. K. Bhartia, and Z. Ahmad, Properties of Mount Pinatubo aerosols as derived from Nimbus-7 total ozone mapping spectrometer measurements, *J. Geophys. Res.*, **100**, 14,043–14,055, 1995.
- Torres, O., P. K. Bhartia, J. R. Herman, Z. Ahmad, and J. Gleason, Derivation of aerosol properties from satellite measurements of backscattered ultraviolet radiation: Theoretical basis, *J. Geophys. Res.*, **103**, 17,099–19,110, 1998.
- D. R. Allen, Department of Geophysical Sciences, University of Chicago, 5734 S. Ellis Ave., Chicago, IL 60637. (drallen@bethel.uchicago.edu)
- M. R. Schoeberl and J. R. Herman, NASA Goddard Space Flight Center, Code 916, Greenbelt, MD 20771.

(Received January 6, 1999; revised July 8, 1999; accepted July 15, 1999.)